Nuclear Engineering and Technology 52 (2020) 1380–1385

Contents lists available at ScienceDirect

Nuclear Engineering and Technology

journal homepage: www.elsevier.com/locate/net

Original Article

Optimization of outer core to reduce end effect of annular linear induction electromagnetic pump in prototype Generation-IV sodium-cooled fast reactor

Jaesik Kwak, Hee Reyoung Kim*

Ulsan National Institute of Science and Technology, 50, UNIST-gil, Ulsan, 44919, Republic of Korea

ARTICLE INFO

Article history:
Received 26 July 2019
Received in revised form
27 November 2019
Accepted 9 December 2019
Available online 11 December 2019

Keywords:
Annular linear induction electromagnetic pump
Electromagnetic field
Maxwell's equation
End effects
Numerical analysis method
PGSFR

ABSTRACT

An annular linear induction electromagnetic pump (ALIP) which has a developed pressure of 0.76 bar and a flow rate of 100 L/min is designed to analysis end effect which is main problem to use ALIP in thermohydraulic system of the prototype generation-IV sodium-cooled fast reactor (PGSFR). Because there is no moving part which is directly in contact with the liquid, such as the impeller of a mechanical pump, an ALIP is one of the best options for transporting sodium, considering the high temperature and reactivity of liquid sodium. For the analysis of an ALIP, some of the most important characteristics are the electromagnetic properties such as the magnetic field, current density, and the Lorentz force. These electromagnetic properties not only affect the performance of an ALIP, but they additionally influence the end effect. The end effect is caused by distortion to the electromagnetic field at both ends of an ALIP, influencing both the flow stability and developed pressure. The electromagnetic field distribution in an ALIP is analyzed in this study by solving Maxwell's equations and using numerical analysis.

1. Introduction

Electromagnetic pumps were developed as a method for transporting molten metal at the beginning of the 20th century in the Soviet Union. After much theoretical analysis, experiments, and verification of electromagnetic pumps, research and development on using electromagnetic pumps for transporting liquid metal coolant such as sodium in nuclear reactors was started with the aim of commercializing large capacity pumps. The important advantages of using an electromagnetic pump as a thermohydraulic system of nuclear reactors include its simple structure, easy control, safety, and low-maintenance [1]. Firstly, there is no moving part that is directly in contact with the liquid, such as the rotating blades of a mechanical pump; therefore, an electromagnetic pump has advantages in safely transporting sodium, considering the high temperature and reactivity of liquid sodium. Secondly, electromagnetic pumps have a simple structure of a coil-wrapped pipe; they are based on a simple operating theory, and hence, there is a low possibility of a failure; they are easy to troubleshoot from a maintenance viewpoint. Because of this simple operating theory, their performance can be controlled easily as the output is proportional to the input power [2].

Electromagnetic pumps with these advantages and characteristics can be divided into conduction and induction types depending on how they generate the Lorentz forces that transport electrically conductive liquid metals [3]. Both types of electromagnetic pump operate on the same basic principle of allowing the current and magnetic fields to intersect each other within a liquid metal, producing a thrust in a direction perpendicular to the fields to drive the liquid metal. In the case of a conduction electromagnetic pump, a direct current is sent through an electrode in contact with the liquid metal from an external power source, and a magnetic field must be provided separately. However, an induction electromagnetic pump is used mainly because of the advantage of requiring only a single power device to simultaneously provide current and magnetic fields. It achieves this by discharging a current in the liquid metal without an electrode through the use of a single or multi-phase alternating current. Induction electromagnetic pumps can be divided into rectangular or annular sections depending on the geometric form of the flow path through which liquid metal passes. In the case of rectangular cross-sectional types, pump performance tends to be further reduced because of the

* Corresponding author.
E-mail address: kimhr@unist.ac.kr (H.R. Kim).

https://doi.org/10.1016/j.net.2019.12.006

transversal edge effect that appears geometrically in addition to the end effect on both ends of the electromagnetic pump [4]. Because of these reasons, an annular linear induction electromagnetic pump (ALIP) is considered for transporting large quantities of liquid metal in a stable manner such as for the thermohydraulic system of a nuclear reactor [5].

For the analysis of an ALIP, some of the most important characteristics are related to the electromagnetic properties such as the magnetic field, current density, and Lorentz force. These electromagnetic properties not only affect the performance of an ALIP, but also affect the end effect. The end effect is caused by the distortion of the electromagnetic field at both ends of an ALIP, influencing both the flow stability and developed pressure [6,7]. An ALIP which has a developed pressure of 0.76 bar and a flow rate of 100 L/min is designed to analysis end effect which is main problem to use ALIP in thermohydraulic system of the prototype generation-IV sodium-cooled fast reactor (PGSFR). In this study, the electromagnetic field distributions in the components of an ALIP are analyzed by solving Maxwell's equations and using numerical analysis.

2. Theoretical approach

A basic model of an ALIP is designed as shown in Fig. 1, and it is divided into two main areas [2]. The first area is the flow path in the form of an annular cross section in which the liquid metal is present between the inner and outer pipes. In this case, the pipe is made of SUS 316, taking the reactivity of the liquid metal, the distortion prevention of the magnetic field, and the physical strength into account. The second area is an electromagnet area consisting of internal and external magnet cores and coils. The main purpose of this area is to create a square magnetic field in the form of a sine wave, using silicon steel plates with strong magnetic permeability and copper with low electrical resistance. Laminated, thin, silicon steel plates and oxygen-free electrolytic copper are chosen to reduce energy loss attributed to Ohm's law. When the three-phase current is properly arranged through the windings of the copper coils, a magnetic field is formed as a sinusoidal wave and moves axially. It travels along the inner core and is induced into the teeth of the outer core in the shape of E, forming a radial magnetic field.

In the flow path, when the above magnetic field is formed, the circumferential current is induced by Faraday's law from the axial magnetic field. As a result, an axial Lorentz force is generated as a cross-product of the radial magnetic field and the circumferential current density.

The two main areas of an ALIP have resistance caused by the windings of the electrical conductor coil, magnetizing reactance necessary to generate a Lorentz force, leakage reactance, and resistive components caused by the conductive liquid metal. The ALIP is connected to three-phase power, and each phase is electrically 120° apart. Because the absolute value of amplitude is equal in the three phases, it can be assumed that the results are obtained after considering the case of one phase in the design analysis.

The electromagnetic relationships between the magnetic field, current density, and Lorentz force are derived from Maxwell's equation, which is composed of Ampère's law, Faraday's law, and Gauss's law for magnetism as represented in Eqs. (1)–(3) [8,9].

$$Ampere's\ law:\ \nabla \times H = J \tag{1}$$

$$Faraday's\ law:\ \nabla \times E = -\frac{\partial B}{\partial t} \tag{2}$$

$$Gauss's\ \text{law for magnetism:}\ \nabla \cdot B = 0 \tag{3}$$

The electric field (E), magnetic field (B), and current density (J) that are applied by the copper coils are represented by considering the 3-phase alternating current, and these have time varying sinusoidal forms, as shown by Eq. (4).

$$E(r,\theta,z) = Re\left[(E_r\hat{r} + E_\theta\hat{\theta} + E_z\hat{z})e^{iwt}\right]$$

$$B(r,\theta,z) = Re\left[(B_r\hat{r} + B_\theta\hat{\theta} + B_z\hat{z})e^{iwt}\right]$$

$$J(r,\theta,z) = Re\left[J_\theta e^{iwt}\right]\hat{\theta} \tag{4}$$

Considering the ideal analysis model of the ALIP as cylindrical coordinates, Eq. (5) is derived from Eq. (1) by applying the curl operation. Because there are only circumferential components for the current density in the coil arrangements, Eq. (5) can be represented as Eq. (6).

$$\nabla \times B = Re\left[e^{iwt}\right]\left[\times \left(\frac{1}{r}\frac{\partial B_z}{\partial \theta} - \frac{\partial B_\theta}{\partial z}\right)\hat{r} + \left(\frac{\partial B_r}{\partial z} - \frac{\partial B_z}{\partial r}\right)\hat{\theta} + \frac{1}{r}\left(\frac{\partial (rB_z)}{\partial r} - \frac{\partial B_r}{\partial \theta}\right)\hat{z}\right] \tag{5}$$

$$\mu J_\theta = \frac{\partial B_r}{\partial z} - \frac{\partial B_z}{\partial r} \tag{6}$$

Eq. (7) is derived from Eq. (2) in a similar way while the right side of Faraday's law is developed as Eq. (8). Considering the axial symmetry of the ALIP, Eq. (7) and Eq. (8) can be combined and rearranged as Eq. (9). Applying Eq. (9) into Eq. (6) produces Eq. (10), which is the relationship between the circumferential component of current density and the induced electric field in the flow path.

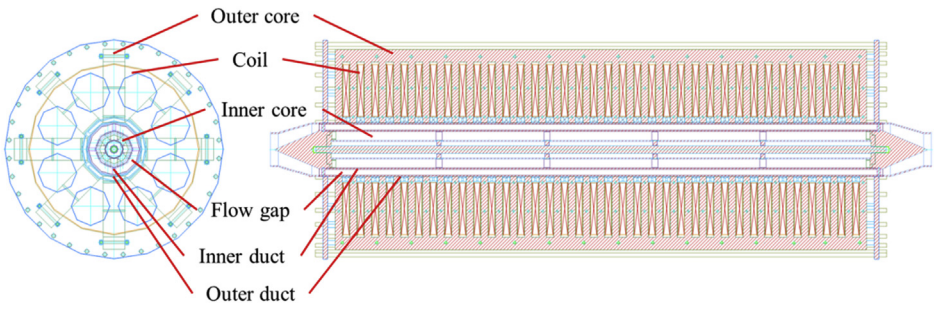

Fig. 1. Cross section of the ALIP.

$$\nabla \times E = Re\left[e^{iwt}\right]\left[\times \left(\frac{1}{r}\frac{\partial E_z}{\partial \theta} - \frac{\partial E_\theta}{\partial z}\right)\hat{r} + \left(\frac{\partial E_r}{\partial z} - \frac{\partial E_z}{\partial r}\right)\hat{\theta} + \frac{1}{r}\left(E_z + r\frac{\partial E_z}{\partial r} - \frac{\partial E_r}{\partial \theta}\right)\hat{z}\right] \tag{7}$$

$$-\frac{\partial B}{\partial t} = -iw(B_r\hat{r} + B_\theta\hat{\theta} + B_z\hat{z})Re\left[e^{iwt}\right] \tag{8}$$

$$\frac{\partial E_\theta}{\partial z} = iwB_r, \frac{\partial E_r}{\partial z} - \frac{\partial E_z}{\partial r} = -iwB_\theta, \frac{1}{r}\left(E_z + r\frac{\partial E_z}{\partial r}\right) = -iwB_z \tag{9}$$

$$\mu J_\theta = \frac{\partial B_r}{\partial z} - \frac{\partial B_z}{\partial r} = \frac{1}{iw}\left(\frac{\partial^2 E_\theta}{\partial z^2} + \frac{\partial\left(\frac{1}{r}\left(E_z + r\frac{\partial E_z}{\partial r}\right)\right)}{\partial r}\right) = \frac{1}{iw}\left(\frac{\partial^2 E_\theta}{\partial z^2} - \frac{1}{r^2}E_z + \frac{1}{r}\frac{\partial E_z}{\partial r} + \frac{\partial^2 E_z}{\partial r^2}\right) \tag{10}$$

Considering the ideal analysis model of the ALIP as cylindrical coordinates, Eq. (11) is derived from Eq. (3) by applying the divergence operation. Eq. (12) and Eq. (13) represent the magnetic field in the radial and axial directions and are derived from Eq. (6) and Eq. (10), respectively.

$$\frac{1}{r}\left(B_r + r\frac{\partial B_r}{\partial r}\right) + \frac{\partial B_z}{\partial z} = 0 \tag{11}$$

$$\frac{\partial}{\partial r}\frac{1}{r}\left(B_r + r\frac{\partial B_r}{\partial r}\right) + \frac{\partial^2 B_r}{\partial z^2} = \mu\frac{\partial J_\theta}{\partial z} \tag{12}$$

$$\frac{1}{r}\frac{\partial B_z}{\partial r} + \frac{\partial^2 B_z}{\partial r^2} + \frac{\partial^2 B_z}{\partial z^2} = -\mu\left(\frac{1}{r}J_\theta + \frac{\partial J_\theta}{\partial r}\right) \tag{13}$$

As shown in Fig. 2, the 3-phase alternating currents in the coils have different phases according to their position and are represented by Eq. (14), which is the optimized arrangement to form the travelling magnetic field [10].

$$J_\theta(z) = \begin{cases} J_\theta Re\left[e^{iwt}\right] & (z_{6n+1,t} \le z \le z_{6n+1,b}) \\ -J_\theta Re\left[e^{iwt-\frac{4}{3}\pi}\right] & (z_{6n+2,t} \le z \le z_{6n+2,b}) \\ J_\theta Re\left[e^{iwt-\frac{2}{3}\pi}\right] & (z_{6n+3,t} \le z \le z_{6n+3,b}) \\ -J_\theta Re\left[e^{iwt}\right] & (z_{6n+4,t} \le z \le z_{6n+4,b}) \\ J_\theta Re\left[e^{iwt-\frac{4}{3}\pi}\right] & (z_{6n+5,t} \le z \le z_{6n+5,b}) \\ -J_\theta Re\left[e^{iwt-\frac{2}{3}\pi}\right] & (z_{6n+6,t} \le z \le z_{6n+6,b}) \end{cases} \quad \text{where} n = 0,1,2,3,4 \tag{14}$$

Based on the above design conditions, 3D modeling and characteristic analysis of the ALIP was performed using a numerical analysis program. The properties of the silicon steel plate and other materials are shown in Fig. 3 and Table 1.

3. Results and discussion

Table 2 and Fig. 4 show the design specifications of an ALIP with

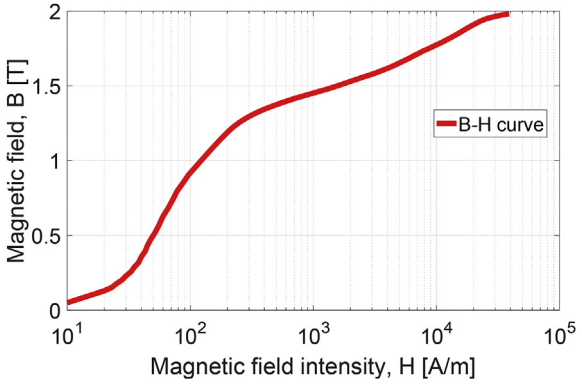

Fig. 3. B–H curve of core (silicon steel plate). (For interpretation of the references to colour in this figure legend, the reader is referred to the Web version of this article.)

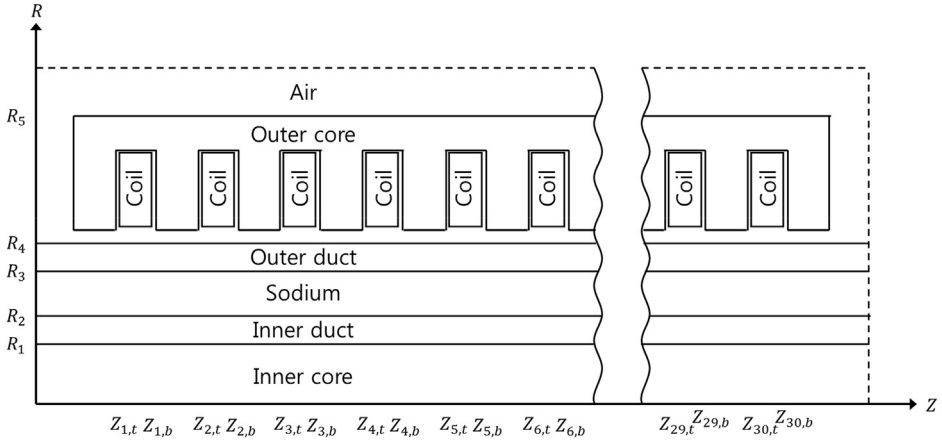

Fig. 2. Boundary conditions model of the ALIP.

Table 1
Properties of materials in the ALIP 3D modeling.

Component	Material	Properties		
		Electrical conductivity [Siemens/m]	Density [kg/m^3]	Relative permeability
Core	35PN250	1.81 E+06	7872	–
Duct	SUS 316	1.35 E+06	8055	1
Flow gap	Sodium	5.18 E+06	878	1
Coil	Copper	2.56 E+07	8933	1
Near the ALIP	Air	0	1.161	1

a flow rate of 100 L/min and a developed pressure of 0.76 bar. Fig. 5 and Fig. 6 shows the schematic diagram and installed an ALIP thermohydraulic experiment to measure electromagnetic properties such as magnetic field and Lorenz electromagnetic force.

The theoretical and experimental values of the distribution of Lorenz electromagnetic force on the end effect characteristics of an ALIP is compared and analyzed as shown in Figs. 7–9. The theoretical calculation confirms that the Lorenz electromagnetic force to be about 30% strong near tooth of the outer core due to the increase in the local magnetic field. However, magnitude of Lorenz force near tooth of the outer core does not appear clearly through the experimental measurement results. The distortion of magnetic field near both ends of an ALIP causes a significant reduction in the Lorenz electromagnetic force, specially near the inlet. The quantity of loss due to end effects is calculated around 10% in terms of the total Lorenz electromagnetic force. It can be seen that the Lorenz electromagnetic force of the reverse direction is generated by the

Table 2
Design specification of the ALIP.

	Design variables	Unit	Values
Hydrodynamic	Flow rate	[L/min]	100
	Developed pressure	[bar]	0.76
	Temperature	[°C]	340
	Velocity	[m/s]	7.152
	Slip	[%]	38.8
	Reynolds number		64778
	Head loss	[bar]	0.116
Geometrical	Core length	[mm]	389.7
	Outer core diameter	[mm]	185.0
	inner core diameter	[mm]	17.1
	Inter core gap	[mm]	7.45
	Flow gap	[mm]	3.15
	Inner duct thickness	[mm]	1.65
	Outer duct thickness	[mm]	1.65
	Slot width	[mm]	18.86
	Slot depth	[mm]	51.48
	Core depth	[mm]	76.48
	Core thickness	[mm]	25.0
	Stacked coil thick	[mm]	33.0
	Coil support ring	[mm]	5.0
	Space in slot depth	[mm]	13.5
	Tooth width	[mm]	12.6
	Slot pitch	[mm]	31.4
	Conductor width	[mm]	7.5
	Conductor thickness	[mm]	1.70
	Insulator thickness	[mm]	0.50
Electrical	Input current	[A]	39
	Input voltage	[V]	30
	Impedance	[Ohm]	0.769
	Input VA	[kVA]	2.03
	Input power	[kW]	0.90
	Power factor	[%]	44.1
	Goodness factor		1.3
	Pole pitch	[mm]	97.4
	Number of slot	[#]	12
	Turns/slot	[#]	30
	Number of pole pairs	[#]	2
	Slot/phase/pole	[#]	1

Table 3
The Number of coil turns for linear grading over 1 pole pitch at both ends.

Slot number	Number of coil turns
1 and 12	12
2 and 11	18
3 and 10	24
4–9	30

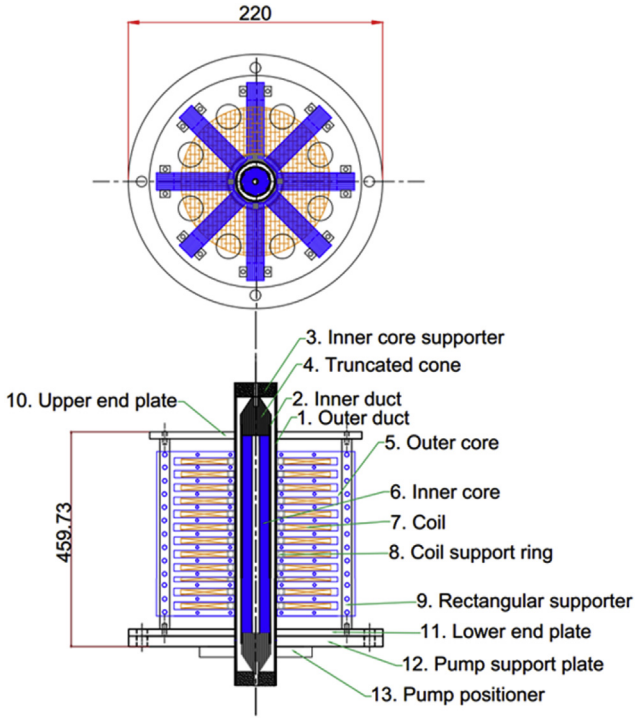

Fig. 4. Design of the ALIP

end effect at the entrance of the electromagnetic pump, and the absolute quantity of reverse Lorenz electromagnetic force through theoretical calculation is 2%.

The reduction graph in Figs. 7–12 means results of optimized an ALIP to reduce end effects by linear grading (see Table 3) methods which decrease turns of winding in the both ends of ALIP. In that case, the quantity of distorted magnetic field is decreased that cause decrease or removal of Lorenz electromagnetic force of the reverse direction. The input voltage and current conditions become different for the same conditions of input power while linear grading of winding make resistance of an ALIP small.

Unlike the data calculated and measured from the same input power values of the normal ALIP design, it is found that in the case of an ALIP with linear grading, there is no reverse Lorenz

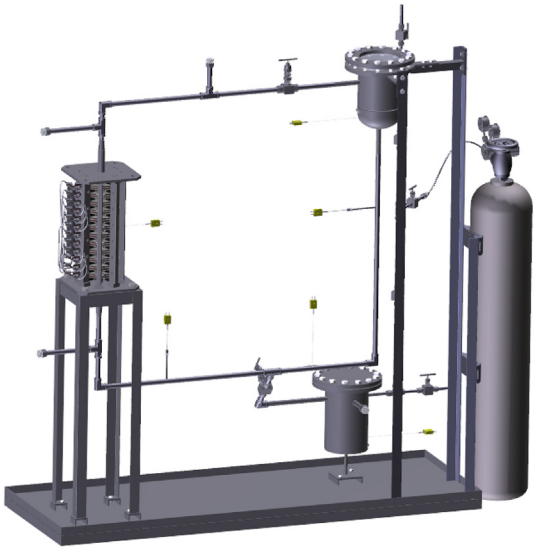

Fig. 5. Schematic diagram of ALIP thermohydraulic experiment.

Fig. 6. ALIP thermohydraulic test bed.

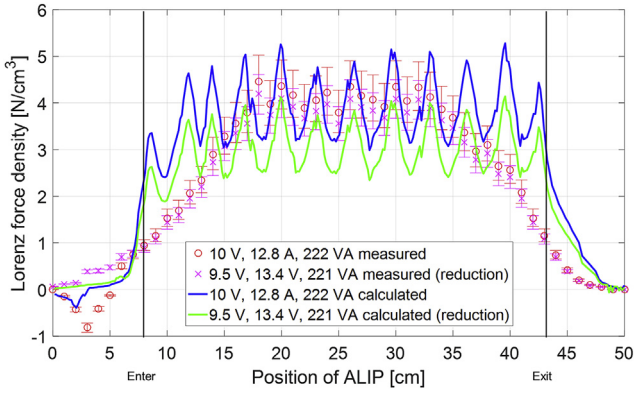

Fig. 7. Lorenz force distribution of the ALIP in the both normal and reduction cases near 222 VA

electromagnetic force from the flow path near the entrance and exit due to magnetic field distortion.

Theoretically, it was expected that the overall loss of Lorenz electromagnetic force due to the linear grading would occur up to 20% or less, but the data from the experimental values in Figs. 7-9 show that the loss of the Lorenz electromagnetic force on the flow path occur up to 10% and a loss of 6% with the average data. On

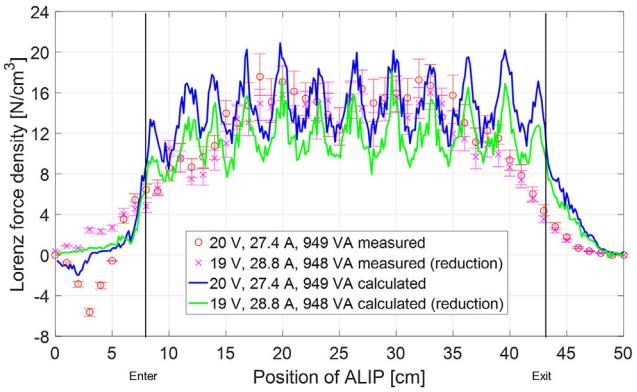

Fig. 8. Lorenz force distribution of the ALIP in the both normal and reduction cases near 949 VA

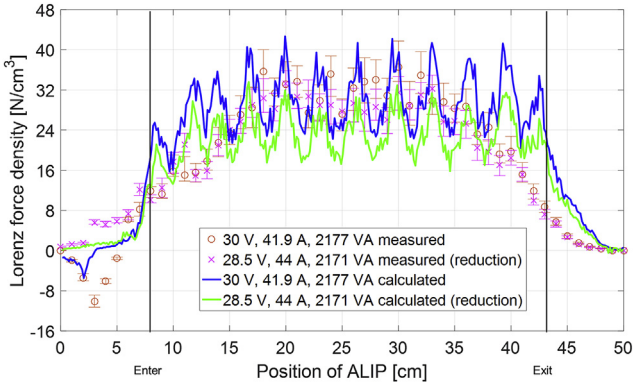

Fig. 9. Lorenz force distribution of the ALIP in the both normal and reduction cases near 2177 VA

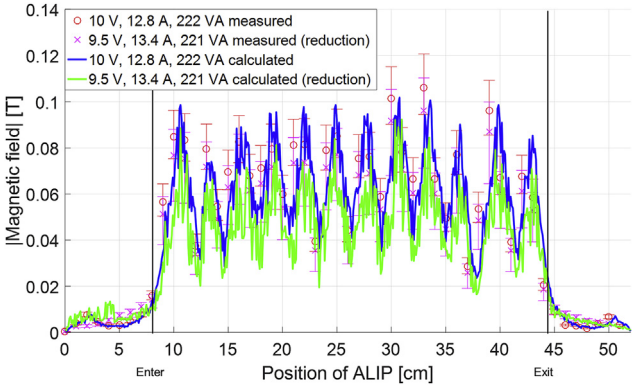

Fig. 10. Magnetic field distribution of the ALIP in the both normal and reduction cases near 222 VA

the other hand, it has been found that the reverse Lorenz electromagnetic force, which occurred at the entrance considered a loss of 2% of the total Lorenz electromagnetic force, is converted into a forward Lorenz electromagnetic force in a similar size by a reduced design, which can be calculated by increasing efficiency by around 4%.

With the end effect of the ALIP, the theoretical calculation and experimental comparative analysis of the strength of the magnetic field are performed and summarized as shown in Fig. 10-12. It can be confirmed that the strength of the magnetic field of the internal flow path of an ALIP has a value of 50% greater than the value of the

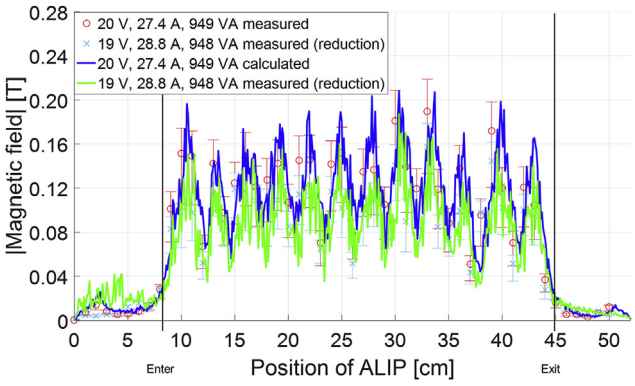

Fig. 11. Magnetic field distribution of the ALIP in the both normal and reduction cases near 949 VA

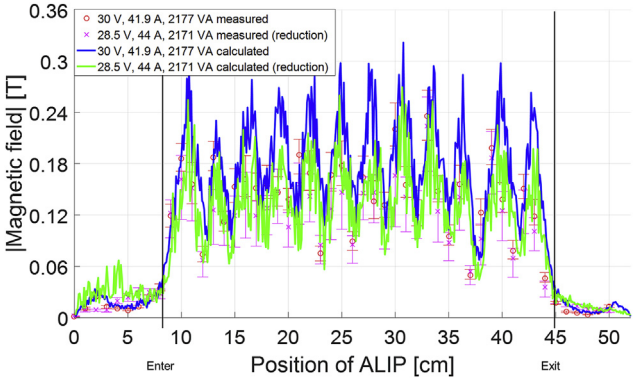

Fig. 12. Magnetic field distribution of the ALIP in the both normal and reduction cases near 2177 VA

slot position of the outer cores, and the errors of the theoretical calculation and experiment are well matched within 15%. In addition, in the range of magnetic fields not exceeding 0.02 T outside the entrance and exit, the error was around 8% or less. Therefore, it is possible to verify that the reduction and distortion of the magnetic field outside the entrance of an ALIP are caused by magnetic field distortion in the experimental and theoretical calculations. It can be seen that peak which is generated by the distortion of magnetic fields at both ends do not occur in the data of the reduced design, which results have same conclusion as similar to cases in Figs. 7-9.

Although the Lorenz force with normal grading was greater by about 2% than with linear grading, it was found that the drawback caused by backward Lorentz force was decreased when the linear grading was applied [11]. In the viewpoint of flow stability in the cooling system of nuclear reactor, end effect which cause sodium vortex in the flow must be decreased even accepting a slight loss of pump efficiency [12].

4. Conclusions

The magnetic field distribution of an electromagnetic pump with a flow rate of 100 L/min and a developed pressure of 0.76 bar was analyzed leading to the optimization of its outer core. A decrease in its strength was accompanied by the saturation of the radial component of the magnetic field in the flow gap. This was caused by the distortion of the radial component of the magnetic field in the flow gap at both ends of an ALIP; this phenomenon is called the end effect. In addition, the generation of a backward developed pressure was observed. To decrease the backward developed pressure, the magnetic field distribution was analyzed for various coil windings. It was confirmed that a linear grading of the coils was effective in weakening the magnetic field at both ends of an ALIP, leading to a decrease of the end effect.

Declaration of competing interest

There are no conflicts of interest to declare without Acknowledgements.

Acknowledgements

This research was supported by the National Nuclear R&D program funded by Ministry of Science and ICT and by the National Nuclear R&D program (NRF-2019M2D1A1067205) and Korea Electric Power Corporation. (Grant number: R18XA06-26) organized by the National Research Foundation (NRF) of South Korea in support of the Ministry of Science and ICT.

References

[1] K. Aizawa, et al., Electromagnetic pumps for main cooling systems of commercialized sodium-cooled fast reactor, J. Nucl. Sci. Technol. 48 (3) (2011) 344–352.
[2] H.R. Kim, The design and fabrication of a small MHD pump for liquid sodium circulation, Ann. Nucl. Energy 73 (2014) 162–167.
[3] J.P. Verkamp, R.G. Rhudy, Electromagnetic Alkali Metal Pump Research Program, GENERAL ELECTRIC CO CINCINNATI OH, 1966.
[4] D.H. Hahn, Advanced SFR design concepts and R&D activities, Nucl. Eng. Technol. 41 (4) (2009) 427–446.
[5] E. Koroteeva, et al., Numerical modeling and design of a disk-type rotating permanent magnet induction pump, Fusion Eng. Des. 106 (2016) 85–92.
[6] H. Araseki, et al., Double-supply-frequency pressure pulsation in annular linear induction pump, part II: reduction of pulsation by linear winding grading at both stator ends, Nucl. Eng. Des. 200 (3) (2000) 397–406.
[7] C.O. Maidana, J.E. Nieminen, First studies for the development of computational tools for the design of liquid metal electromagnetic pumps, Nucl. Eng. Technol. 49 (1) (2017) 82–91.
[8] S.A. Nasar, Linear Motion Electric Machines, John Wiley & Sons, New York, 1976.
[9] D.K. Cheng, Fundamentals of Engineering Electromagnetics, Pearson Education, 1993.
[10] J. Kwak, H.R. Kim, Magnetic field analysis of an electromagnetic pump for sodium thermohydraulic test in the sodium test loop for safety simulation and assessment—phase 1, Prog. Nucl. Energy 101 (2017) 235–242.
[11] C.O. Maidana, J.E. Nieminen, Software development and multiphysics analysis of liquid metal annular linear induction pumps, in: 15th International Energy Conversion Engineering Conference, 2017.
[12] H. Araseki, et al., Magnetohydrodynamic instability in annular linear induction pump: Part I. Experiment and numerical analysis, Nucl. Eng. Des. 227 (1) (2004) 29–50.